technical note technical note

Sources of Variability in Fire Test Data: A Case Study on Poly(aryl ether ether ketone)

December 2012

DOT/FAA/TC-TN12/42

U.S. Department of Transportation
Federal Aviation Administration

NOTICE

This report is available at the Federal Aviation Administration William J. Hughes Technical Center's Full-Text Technical Reports page: actlibrary.tc.faa.gov in Adobe Acrobat portable document format (PDF).

Technical Report Documentation Page

1. Report No.	2. Government Accession No.	3. Recipient's Catalog No.
DOT/FAA/TC-TN12/42		

4. Title and Subtitle	5. Report Date
SOURCES OF VARIABILITY IN FIRE TEST DATA: A CASE STUDY ON POLY(ARYL ETHER ETHER KETONE)	December 2012
	6. Performing Organization Code

7. Author(s)	8. Performing Organization Report No.
Ezgi S. Oztekin[1], Sean B. Crowley[2], Richard E. Lyon[2], Stanislav I. Stoliarov[3], Parina Patel[4], and T. Richard Hull[4]	

9. Performing Organization Name and Address	10. Work Unit No. (TRAIS)
[1]Technology and Management International, LLC (TAMI) 1433 Hooper Ave, Suite 330 Toms River, NJ 08753 [2]U.S. Department of Transportation Federal Aviation Administration William J. Hughes Technical Center Atlantic City International Airport, NJ 08405 [3]Department of Fire Protection Engineering University of Maryland College Park, MD 20742 [4]Centre for Fire and Hazards Science School of Forensic and Investigative Science University of Central Lancashire Preston, PR1 2HE, UK	11. Contract or Grant No.

12. Sponsoring Agency Name and Address	13. Type of Report and Period Covered
U.S. Department of Transportation Federal Aviation Administration Northwest Mountain Region − Transport Airplane Directorate 1601 Lind Avenue, SW Renton, WA 98057	Technical Note
	14. Sponsoring Agency Code ANM-115

15. Supplementary Notes

The Federal Aviation Administration William J. Hughes Technical Center Aviation Research Division COR was Richard E. Lyon.

16. Abstract

In an effort to minimize uncertainties seen in bench scale tests, the sources of variability in fire test data were investigated. An earlier study—a PhD thesis written by Patel at the University of Central Lancaster, UK, in 2011 titled "Investigation of Fire Behavior of PEEK-based Polymers and Compounds"—on poly(arly ether ether ketone) (PEEK) showed that the fire performance parameters of this thermoplastic changed noticeably when exposed to moisture prior to the test. The present research is a follow-up study where a series of cone calorimetry tests were conducted on conditioned PEEK specimens to analyze the previously reported ignition time scatter and its relation to surface bubble formation. Pyrolysis modeling is, subsequently, carried out to relate the moisture content with the model parameters and to explain the possible physical mechanisms that cause the difference in ignition times between wet and dry samples.

17. Key Words	18. Distribution Statement
Variability, Cone calorimetry, Fire-safe polymers, Poly(aryl ether ether ketone) (PEEK), Thermal decomposition, Ignition	This document is available to the U.S. public through the National Technical Information Service (NTIS), Springfield, Virginia 22161. This document is also available from the Federal Aviation Administration William J. Hughes Technical Center at actlibrary.tc.faa.gov.

19. Security Classif. (of this report)	20. Security Classif. (of this page)	21. No. of Pages	22. Price
Unclassified	Unclassified	41	

ACKNOWLEDGEMENTS

The authors would like to thank Natallia Safronava and Richard N. Walters for Mircoscale Combustion Calorimetry and Thermogravimetric Analysis measurements.

TABLE OF CONTENTS

LIST OF FIGURES

LIST OF TABLES

LIST OF SYMBOLS AND ACRONYMS

α	Absorption coefficient
θ	Stoichiometric coefficient
σ	Stefan-Boltzmann constant
ξ	Concentration
$\dot{q}''_{ext}$	External heat flux
$\dot{q}''_{cond}$	Conduction heat flux
A_{exp}	Arrhenius pre-exponential factor
β	Heating rate
c_p	Specific heat capacity
E_a	Arrhenius activation energy
I	Radiative heat flux
I_s	External heat flux
J_g	Species-mass flux
k	Thermal conductivity
k′	Arrhenius rate coefficient
L	Characteristic length scale
α_m	Mixture radiation absorption coefficient
D_m	Mixture diffusivity
K_m	Mixture conductivity
η	Heat release capacity
P	Polymer
P_{bubble}	Bubbled polymer
P_{melt}	Molten polymer
ρ	Density
R	Gas constant
r_r	Reaction rate
ign	Ignition property
ign_{wet}	Property of wet polymer
ign_{dry}	Property of dry polymer
T	Temperature
t	Time
t_{start}	Start time
t_{end}	End time
T_∞	Ambient temperature
T_g	Glass transition temperature
T_g	Gas temperature
T_m	Melting temperature
T_{avg}	Average temperature

AHRR	Average heat release rate
ASTM	American Society for Testing and Materials
EHOC	Effective heat of combustion
HOC	Heat of combustion
HRR	Heat release rate
MCC	Microscale Combustion Calorimetry
MLR	Mass loss rate
PEEK	Poly(aryl ether ether ketone)
PHRR	Peak heat release rate
TGA	Thermogravimetric analysis
THR	Total heat release

EXECUTIVE SUMMARY

In an effort to minimize uncertainties seen in bench scale tests, the sources of variability in fire test data were investigated. An earlier study on poly(aryl ether ether ketone) (PEEK) showed that the fire performance parameters of this thermoplastic changed noticeably when exposed to moisture prior to test. The present research is a follow-up study where a series of cone calorimetry tests were conducted on conditioned PEEK specimens to analyze the previously reported ignition time scatter and its relation to surface bubble formation. Pyrolysis modeling was, subsequently, carried out to relate the moisture content with the model parameters and to explain the possible physical mechanisms that caused the difference in ignition times between wet and dry samples.

INTRODUCTION

The study of fire behavior is interdisciplinary with combustion, turbulence, radiation, and material science each playing equally important roles. There are unknowns associated with each of these individual disciplines and with their complex interactions. Furthermore, fire is a transient phenomenon; both the fuel source and the area of interest alter their form and state during the course of fire, introducing additional ambiguities. These lead to scenario-specific fire behavior and, when combined with the variations in the test conditions and fuel properties, result in a wide range of uncertainty in large-scale fire tests. In fact, even for the bench scale tests that are comparably easier to conduct in a controlled environment, the reproducibility of the data can be low. For example, Patel has recently reported a wide scatter in cone calorimetry test results for poly(aryl ether ether ketone) (PEEK) [1]. Both the ignition times and the average heat release rates (HRR) were found to be sensitive to the moisture absorption of the tested specimen (see figure 1). Although the effect of moisture on the burning behavior has long been recognized [2-5], the amount of moisture in these studies was appreciably (at least an order of magnitude) higher than that which is possible for PEEK. The supplier of the material lists the maximum water desorption of PEEK to be 0.26% when heated to 125°C for 24 hours [6]. Yet, under the same test conditions, approximately 2-minute variations were found in ignition times between specimens of varying moisture uptakes [1]. It is interesting that such a small amount of water (or its lack thereof) has such an impact on fire behavior. It is also intriguing that, unlike cellulosic materials, for which moisture delays ignition [2], PEEK ignites earlier when exposed to moisture. Time to ignition, which is important because it is a measure of not only fire initiation but also of fire growth [7], is the main focus of this research. The cone calorimetry tests of PEEK are analyzed in an attempt to understand the variability in ignition delays observed in bench scale tests. Fire performance parameters (e.g., heat release rate (HRR), total heat release (THR), mass loss, effective heat of combustion, and ignition time) are examined at three heat flux settings and for varying sample thicknesses. Moreover, the effect of moisture absorption is studied by repeating the experiments for samples with varying moisture content in two groups (i.e., wet and dry). To further investigate the physical phenomena behind the variability of ignition delays of PEEK specimens, the one-dimensional pyrolysis tool ThermaKin [8-10] is employed.

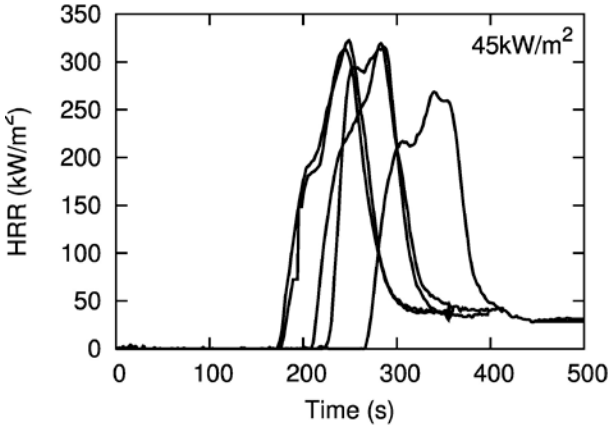

Figure 1. Replicate HRR Measurements of Unconditioned Samples Exposed to the Same External Heat Flux [1]

METHODOLOGY

EXPERIMENTAL SECTION.

MATERIAL.

PEEK has excellent mechanical properties (toughness, strength, and rigidity) and exceptional chemical and radiation resistance at elevated temperatures, and has received considerable attention since its commercial introduction in 1978 by Imperial Chemical Industries. The wide application areas of this semicrystalline, high-performance thermoplastic include industries such as transportation, medical, and food processing. In the aerospace industry, PEEK is used as an aircraft structural material in the exterior and as a cabin material in the interior for its notable mechanical properties, low flammability, and low smoke emission levels. PEEK is a highly aromatic, semicrystalline thermoplastic with a maximum degree of 40% crystallinity [11]. Due to its semicrystalline nature and aromatic structure, it has notable thermal resistance (glass transition and melting temperatures are T_g = 143°C and T_m = 343°C, respectively). The morphological features and thermal properties are widely studied by many researchers [11-17]. However, the majority of these studies characterize the thermal behavior up to the decomposition temperature, and only a few involve the thermal analysis of decomposition kinetics [18-20] and the fire behavior [1, 21, and 22].

In this study, PEEK grade 450G, supplied by VICTREX®, is used. Table 1 shows the property values for VICTREX PEEK 450G polymer at room temperature [6]. The other relevant literature data for PEEK are the average effective heat of flaming combustion (17 kJ/g), the net heat of complete combustion (~30 kJ/g), the ignition temperature, T_{ign} (570°-580°C), and the critical heat flux for ignition, $\dot{q}''_{crit}$ (30-40 kW/m^2) [22-24]. For modeling purposes, the material properties and reaction parameters found in the literature are revisited in the Material Properties and Reaction Parameters sections, respectively.

Table 1. Material Properties of VICTREX PEEK 450G at 23°C [6]

ρ (kg/m^3)	1300
k (W m^{-1} K^{-1})	0.25-0.29
c_p (J kg^{-1} K^{-1})	2160

SAMPLE PREPARATION. The commercially available, injection molding-grade VICTREX PEEK 450G samples were separated into three groups and exposed to different environmental conditions. The first group, classified as dry samples, was kept in a vacuum oven at 100°C. The second group, classified as wet samples, was immersed in distilled water at close to boiling temperature. The last group, classified as ambient samples, was conditioned in standard atmosphere at 21° ±3°C and 50 ±5% in a relative humidity chamber [25]. The moisture contents of samples were measured as the percent weight change. Figure 2 shows the moisture content averaged over nine samples in each classification for 3.9-mm-thick samples plotted as a function of the square root of time. Within 9 days of conditioning, the wet samples reached 0.38% by weight of constant moisture content, while the dry samples lost 0.35% by weight. The difference

in moisture content between the wet and dry samples was 0.73%, while the difference between the ambient and dry samples was 0.35%. Experiments were started after 3 weeks of conditioning, and weight measurements were continued for the samples to be tested. The same conditioning procedure was also followed for 1- and 10-mm-thick specimens. The dry samples represent the moisture-free polymer, while the wet samples are those with the maximum amount of possible moisture uptake for PEEK. The effect of moisture on the burning behavior is bracketed by investigating the thermal response of the material at these two extreme conditions. The fire behavior of the ambient samples should be between dry and wet samples.

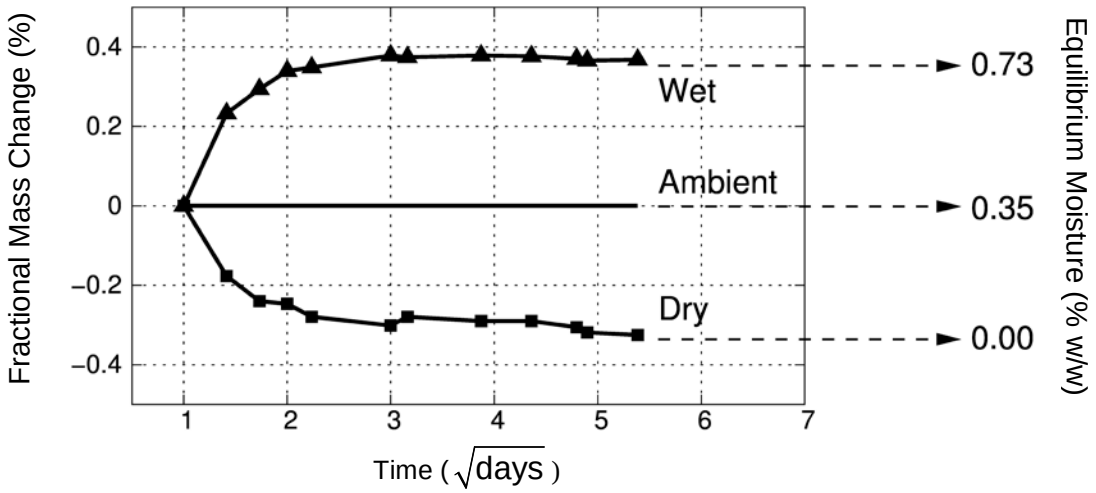

Figure 2. Time Variation of Moisture Content in Terms of Percentage Mass Change, $(m-m_0)/m_0$, for 3.9-mm-Thick Samples in Wet, Ambient, and Dry Environments

THERMAL ANALYSIS.

Microscale Combustion Calorimetry. The complete heat of combustion (HOC) of volatiles of PEEK pyrolysis was obtained using Microscale Combustion Calorimetry (MCC) in accordance with the American Society for Testing and Materials (ASTM) standard [26]. Tests were conducted with a constant heating rate of 1 K/s for mg size specimens punched out of the conditioned 1-mm-thick samples. The results are presented as the average of three tests for wet, ambient, and dry conditioning types. The average char fraction, μ (as %, g/g), specific HRR (in W/g), heat release capacity, η, (in J/gK), peak temperature, T_p, (in °C), and complete HOC (in kJ/g) are shown in table 2. Note that the HOC in table 2 is the HOC of the fuel gases per unit initial mass of solid. Accordingly, the HOC of the volatiles, calculated from the ratio $h_C/(1-\mu)$, is ~25-26 kJ/g.

Table 2. Average Values for Wet, Ambient, and Dry Samples Obtained From MCC

Sample Type	μ (%)	HRR (W/g)	η (J/gK)	T_p (°C)	h_C (kJ/g)
Wet	49	344	364	627	13.4
Ambient	49	332	339	627	12.9
Dry	49	355	375	625	12.6

Thermogravimetric Analysis. Experiments with varying heating rate, β, of 3, 10, and 30°C/min were conducted on ~8.5-mg samples (not conditioned) using a Mettler Toledo TGA/SDTA851[c] thermogravimetric analyzer (TGA). The temperature variation of the mass loss rate (MLR) corresponding to different heating rates is shown in figure 3. The onset of decomposition is between 520° to 590°C. The TGA data are in agreement with the previous reports [18-20]; for β of 30°C/min mass loss starts at 550°C and reaches its maximum at 617°C. By the time it reaches this temperature, almost 35% of the initial mass has already been lost. The 5% mass loss temperature is 577°C. The slower second reaction, apparent from the mass variation with temperature curve (not shown), starts at 627°C, which is a little lower than the reported value in reference 19.

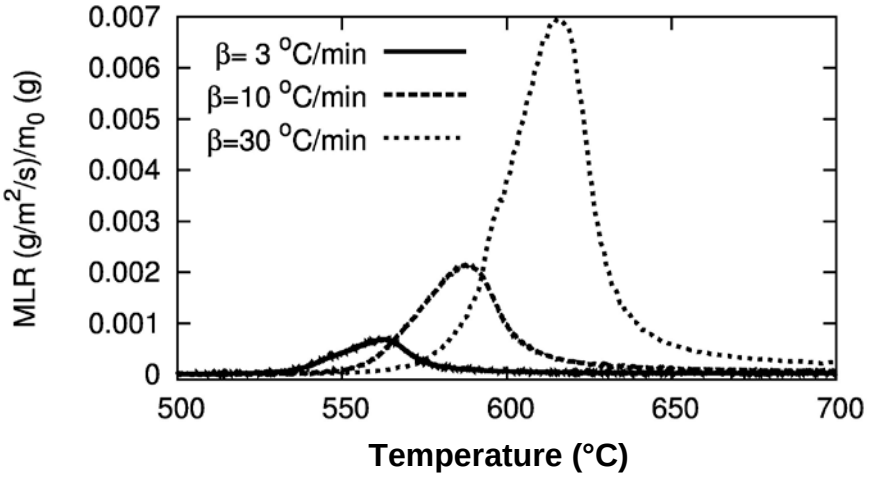

Figure 3. TGA Data: Temperature Variation of MLR for Heating Rates of 3, 10, and 30°C/min

CONE (FIRE) CALORIMETRY. A cone (fire) calorimeter built by Fire Testing Technology Ltd. was used to measure HRR and MLR. The ASTM standard [27] was followed: the heat release measurement was based on oxygen consumption principle, while the mass loss was recorded with a load cell under the material placed in a horizontal position; an edge frame was used to hold the specimen; the polymer was wrapped from below in aluminum foil and Kaowool was placed below the polymer to provide insulation; the distance from the specimen surface to the cone heater was 25 mm and to the igniter was 13 mm; and a Schmidt-Boelter heat flux sensor was used for calibration.

The sample thicknesses studied were 1, 3.9, and 10 mm, with particular attention given to the 3.9-mm-thick samples subject to three external heat fluxes: 50, 70, and 90 kW/m^2. In addition to the main tests of this study, cone calorimetry was also used to correlate material thermal properties (conductivity and heat capacity), and reaction parameters (HOC and char yield), as described in the Material Properties and Reaction Parameters sections, respectively.

NUMERICAL SECTION.

Numerical modeling is performed using the one-dimensional pyrolysis tool, ThermaKin [8-10]. ThermaKin solves governing equations for energy and species mass to study the thermal response of a material exposed to an external heat source. The material is expressed as a one-dimensional object with layers of different components. Each component, categorized as solid, liquid, or gas, has its own set of thermal and optical properties that determine the heat transfer within the condensed phase and interacts with the gas phase. The thermal properties are defined as a function of temperature, while the optical properties are set as constants. The heat conduction is described by Fourier's Law. The convective heat transfer is expressed through Newton's Law of Cooling with a specified convection coefficient at the uninsulated boundaries. The in-depth radiation transfer is computed using a generalized form of Beer-Lambert law. The Arrhenius type of reaction scheme is adapted to couple the energy equation with the species-mass equation. Any number of reactions can be defined between components by specifying the relevant Arrhenius parameters and the heat of decomposition reaction. The lower- and upper-temperature limits can be specified to activate or deactivate reactions, respectively. The ignition criteria is based on critical mass flux. When it is reached, the external heat flux is increased by an amount of flame heat flux to simulate the effects of flame on the material face.

GOVERNING EQUATIONS.

ThermaKin solves the following set of governing equations:

Conservation of gas-phase species mass

$$\frac{\partial \xi_g}{\partial t} = -\frac{\partial J_g}{\partial z} + \sum_{1}^{N_r} \theta_r^g r_r \tag{1}$$

Conservation of condensed-phase species mass

$$\frac{\partial \xi_i}{\partial t} = -\sum_{1}^{N_r} \theta_r r_r \tag{2}$$

Conservation of condensed-phase energy

$$\sum_{i}^{N} \xi_i c_{pi} \frac{\partial T}{\partial t} = -\frac{\partial \dot{q}''_{cond}}{\partial z} + \sum_{1}^{N_r} r_r h_r + \alpha_M I \left(1 - \frac{\sigma_S T^4}{I_S}\right) - \sum_{g}^{N_g} J_g \frac{\partial}{\partial z}\left(\int_0^T c_{pg} dT\right) \quad (3)$$

where $\dot{q}''_{cond} = -\frac{\partial}{\partial z}(k_M \frac{\partial T}{\partial z})$ is the conduction heat flux computed using mixture conductivity k_M; $J_g = -\frac{\partial}{\partial z}(D_M \frac{\partial \xi_g}{\partial z})$ is the species mass flux with mixture diffusivity D_M; and $r_r = \xi_r k'$ is the reaction rate with the Arrhenius rate coefficient, $k' = A\exp(-E_a / RT)$. ξ, c_p, and T are the concentration, heat capacity, and temperature; θ and h are the stoichiometric coefficient and heat of reaction, respectively. α_M and σ_S are the mixture radiation absorption coefficient and Stefan-Boltzmann constant. I_S and I are the external heat flux and the radiation flux inside the material computed using Beer-Lambert law.

BOUNDARY AND INITIAL CONDITIONS. The external heat flux, I_S, is specified at the front face of the material exposed to the radiant heater. The back surface is insulated with 15-mm-thick Kaowool. The I_S flux values are 50, 70, and 90 kW/m^2. The ambient temperature is taken to be 300 K. The flame heat flux is set to 15 kW/m^2. The forced convection due to extraction is neglected because of the large exhaust hood area, hence, the negligible fluid velocities (the exhaust hood area is the cross-sectional area from which the volatiles are drawn inside the exhaust duct vertically). The natural convection heat flux coefficient is estimated to be 10 $W\,m^{-2}\,K^{-1}$ from the simplified horizontal plate correlations for air; for laminar flows $h = 1.32((T_{avg} - T_g)/L)^{(1/4)}$, where L is the characteristic length scale, T_{avg} and T_g are the average solid and gas temperatures with L = 0.1 m, T_{avg} ~600 K and T_g ~300 K. The critical mass flux for ignition is specified as 3x10^{-4} kg m^{-2} s^{-1} at the lower flammability limit (flashpoint). This value is within acceptable range of critical mass flux values found in literature, 1 g/s [28], and produces the measured ignition temperature. The material thicknesses modeled are 1, 3.9, and 10 mm.

MODEL SETUP. Polymers, when exposed to heat undergo physical and chemical processes. The physical changes (such as elongation, melting, and charring) depend on the type of polymer. In thermoplastics, for instance, transition from a solid state to a polymer-melt is determined by the degree of crystallinity. Physical deformation, marked by transition to a rubbery state, starts when the glass transition temperature is reached, and advances to a viscous state with increased temperatures to the melting point [29]. PEEK with 35% crystallinity becomes rubbery at T_g = 143°C and starts flowing at T_m = 343°C. The experiments showed that the difference in ignition times between wet- and dry-PEEK specimens is associated with the onset of melting (see the Surface Temperature Measurements section), suggesting that the glass transition process can be omitted in the modeling efforts for the specific material studied herein.

Based on the TGA data, the thermal decomposition of PEEK is modeled using two successive first-order reactions. The onset temperature is 601°C for the second reaction and the first reaction is governed by the first-order Arrhenius equation (see the Reaction Parameters section). Note that the onset temperature for the second reaction is lower than the value specified in the Thermal Analysis section for β = 30°C/min; this is because lower heating rate data are used in the determination of decomposition kinetics (see the Reaction Parameters section). In modeling, the melting process is also included before degradation, resulting in the following set of reactions: polymer, (P), changes to a polymer-melt (P_{MELT}), which degrades to $Char_A$ and Gas_A of which $Char_A$ subsequently degrades to $Char_B$ and Gas_B. Finally, $Char_B$ oxidizes to Gas_C:

$$P \rightarrow P_{MELT} \quad (4)$$

$$P_{MELT} \rightarrow \mu_A\, Char_A + (1-\mu_A)\, Gas_A \quad (5)$$

$$Char_A \rightarrow \mu_B\, Char_B + (1-\mu_B)\, Gas_B \quad (6)$$

$$Char_B \rightarrow Gas_C \quad (7)$$

where μ_A = 0.62 and μ_B = 0.77, (i.e., the total char yield is 0.48 (=μ_A x μ_B). For the wet samples, the reaction scheme above is modified to replace reaction in equation 5 with reactions in equations 8 and 9 below:

$$P_{MELT} \rightarrow P_{BUBBLE} \quad (8)$$

$$P_{BUBBLE} \rightarrow \mu_A\, Char_A + (1-\mu_A)\, Gas_A \quad (9)$$

Accordingly, for wet samples, once melting starts at T_m, bubbling takes place following a first-order Arrhenius reaction. As the molten polymer, P_{MELT}, transforms to the bubbled polymer, P_{BUBBLE}, its thermal properties change.

DETERMINATION OF MODEL PARAMETERS.

The number of input parameters for pyrolysis modeling can be extensive. In addition to the thermal and optical parameters of each material, the reaction kinetics and their associated heat values are required for the model. Although some of these parameters can be measured with an acceptable uncertainty, most of them are difficult to measure and are approximated based on available laboratory tests. Cone calorimetry test data were used for the temperature-dependent property values, the average effective HOC, and the char yield as outlined in the Material Properties and Reaction Parameter sections. In the determination of reaction kinetics, TGA data were used (see the Reaction Parameters section).

MATERIAL PROPERTIES. Except for the density, which can be measured as the volume and mass of specimens that are readily known, virgin-material properties are determined by fitting model predictions with temperature measurements. The temperature histories at two locations, at the front and back ends of the specimen, are recorded for a 10-mm-thick sample subjected to an

external heat flux of 50 kW/m^2. Model parameters are changed until the temperature estimates are in a reasonable agreement with the measurements. The heat capacity and conductivity are assumed to reach their maximum value at the melting temperature. The density is assumed to be constant. Since ignition delay is shown to depend on the moisture uptake of the material, experiments are performed for both wet and dry samples in triplicates. The procedure is followed in two steps. In step 1, the temperature-dependent material properties are decided up to the point of melting temperature. In step 2, material properties are assumed to be constant between melting and ignition and are determined separately for wet and dry samples. Figure 4 (a and b) shows the temperature measurements for dry and wet specimens at 1 (surface) and 9 mm (back end) into the material. The test data are shown with the symbols in the figures. The material properties found as a result of the data fitting are shown in table 3. The material properties of the wet samples differ from those of the dry samples only after melting occurs.

Note that ignition temperature was measured to be ~543°C in the cone calorimetry experiments (see figure 4 (a and b)). Using h = 10 W m^{-2} K^{-1}, T_{ign} = 816 K, ε = 0.9; critical heat flux, $\dot{q}''_{crit}$, can be calculated from $\varepsilon \dot{q}''_{crit} = h (T_{ign}-T_o) + \sigma_S (T_{ign}^4-T_o^4)$ to be ~30 kW/m^2. This finding was also confirmed by a separate set of cone calorimetry experiments (see the Critical Heat Flux section) and is lower than the minimum literature value.

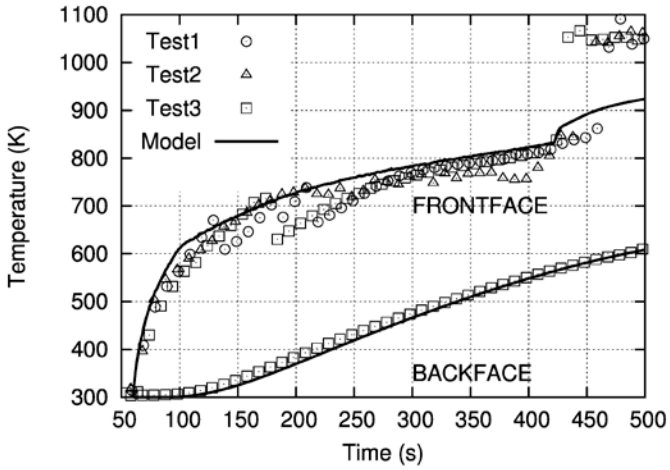

(a) Temperature Histories of Dry Samples

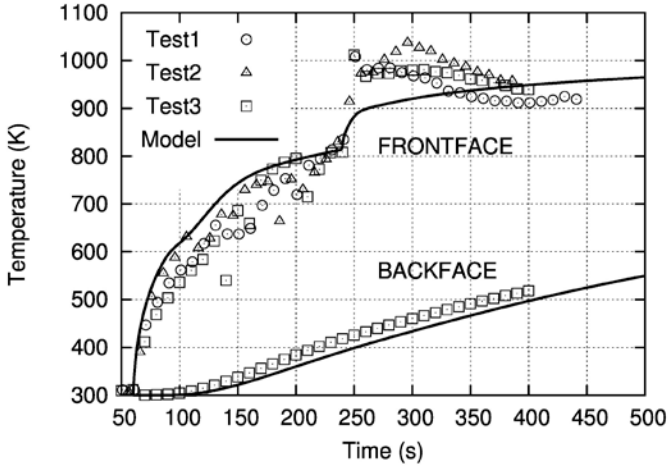

(b) Temperature Histories of Wet Samples

Figure 4. Comparisons of Experimental Data With Model Results

Table 3. Fitted Material Properties

	Fitted Value		
		$T > T_m$	
	$T < T_m$	Dry	Wet
k (W m^{-1} K^{-1})	0.212 +1.26 10^{-4} T	0.29	0.06
c_p (J kg^{-1} K^{-1})	795 +2.22T	2160	1000

Temperature is in Kelvin. T_m (melting temperature) is 616 K.

Edge Frame Effects—The aforementioned 10-mm tests were conducted without edge frames. Edge frames act as a heat sink and reduce the effective value of the external heat flux. The tests were repeated using edge frames to quantify their effects on the measurements. The difference

between model results with and without edge frames is explained by a reduction of 2.5 kW/m^2 in external heat flux.

REACTION PARAMETERS.

Decomposition Kinetics. The pre-exponential factor and the activation energy are decided by fitting ThermaKin results for a fictitious thin sample exposed to heat at both boundaries. The model results are fitted to the TGA data obtained with the heating rate of 10°C/min. The Arrhenius parameters found are E_a = 557,400 (J/mol), $A = 10^{32}$ (1/s) for the first reaction with a char yield of 0.62. The second reaction is specified in two steps with E_a = 89,000 (J/mol), $A = 10^3$ (1/s) for the first step and E_a = 146,500 (J/mol), $A = 10^5$ (1/s), starting from 652°C for the second step with the same char yields of 0.88. The average total char yield is 0.48. The TGA data and model solution showing temperature variation of the mass and the MLR corresponding to β = 10°C/min are shown in figures 5 and 6, respectively.

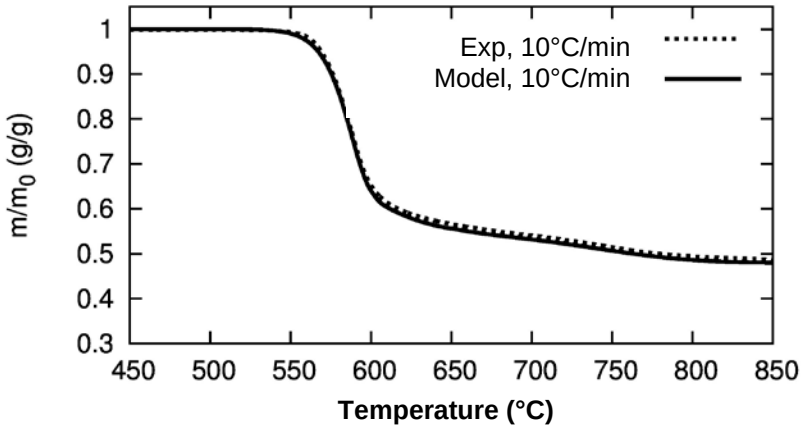

Figure 5. Temperature Variation of Unit Mass at β = 10°C/min, m_o = Initial Mass

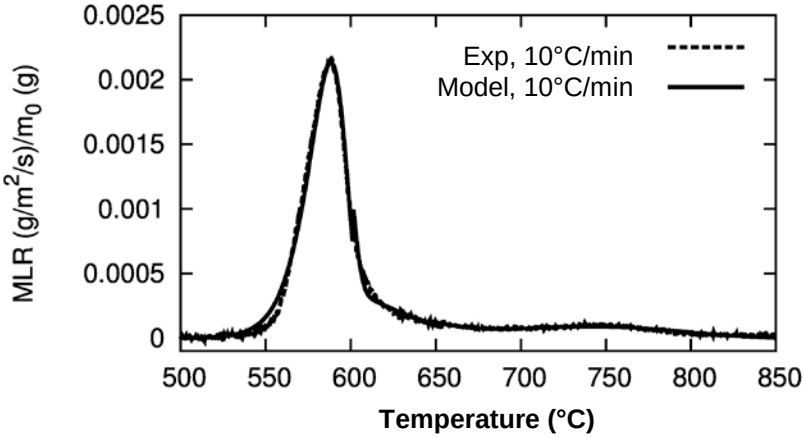

Figure 6. Temperature Variation of MLR at β = 10°C/min

The agreement between the model and test the data deteriorates as the heating rate changes (not shown). Note that the MLR, *dm*/*dt*, depends on the rate of heating, $\beta = dT/dt$. Even if the functional dependency is removed by using the mass loss change as a function of temperature, *dm/dT*, the onset of decomposition will still be different (figure 3 shows ~26 degrees between each heating rate). Hence, the choice of heating rate will alter the ignition temperature. The common practice in the determination of decomposition kinetics is to use TGA data at lower heating rates. This is preferred so that possible measurement errors due to heat transfer effects are minimized [30]. On the other hand, the heating rates of an actual fire are much higher, in the order of 10 to 100 K/s [29]. Note that T_{ign} is an input provided to the model implicitly through the Arrhenius parameters and the critical mass flux. The E_a/A couple is determined by TGA data at 10°C/min since this heating rate and specified critical mass flux provide an ignition temperature close to the experimentally measured value of 543° ±20°C (see figures 4 (a and b) and 10).

Heat of Combustion. The following relation is used to calculate the HOC of volatiles:

$$\dot{Q}_c = \chi \Delta HOC \dot{m} \tag{10}$$

where χ is the combustion efficiency to take into account incomplete combustion. The multiplication term in front of MLR, $\chi\ \Delta HOC$, is called the effective HOC (EHOC). It is simply the ratio of HRR to MLR. In the cone calorimeter analysis program, EHOC is calculated using independent measurements of HRR and MLR.

The EHOC for PEEK, averaged over more than 40 cone calorimetry tests, is approximately 18 kJ/g. This average is lower when only dry sample data are used. Although the difference is small, higher HOC values for wet samples are intriguing because moisture is reported to reduce HOC by diluting the pyrolysis products [31]. It is important to note that the MLR calculated from the recorded mass change of the burning polymer is usually noisy, resulting in erroneous calculations of EHOC. Figure 7 (a) shows example raw data for MLR. More importantly, the EHOC calculation assumes a single reaction, therefore a constant EHOC value. This is a reasonable assumption if the HOC of simultaneous reactions are close to one another. Table 4 shows average EHOC data from cone experiments of 3.9-mm-thick wet and dry samples at three external heat fluxes. The EHOC of dry samples are lower. In addition, the EHOC increases with the heat flux, indicating the contribution from the second reaction.

Table 4. Average Cone Data for 3.9-mm-Thick Samples: HOC

$\dot{q}''_{ext}$ (kW/m^2)	50	70	90
EHOC $_{DRY}$ (kJ/g)	16.6	15.6	18.2
EHOC $_{WET}$ (kJ/g)	19.1	19.5	20.7

The calculations of EHOC for two arbitrarily chosen cone tests are revisited here. Since smoothing raw MLR data removes some of its features (see figure 7 (a)), a piecewise polynomial

curve fit is applied to the mass loss, and the MLR is computed as the derivative of this fitted curve. The EHOC as a function of time is obtained using the ratio of the HRR to the fitted MLR. The calculated EHOC values are shown with symbols in figure 7 (b), and the subscripts show the test number. As shown in the figure, the EHOC is constant at the beginning of the test, but increases 400 seconds into the test. The increase does not mark the initiation of the slow second reaction, but the transition when it starts to dominate. Note that even if the EHOCs are the same for wet and dry samples, this transition may take place at different times, explaining higher average EHOC values for wet samples. In fact, moisture is reported to promote charring reactions, albeit for cellulosic materials [4]. In these experiments, char buildup for wet samples was also observed to occur earlier.

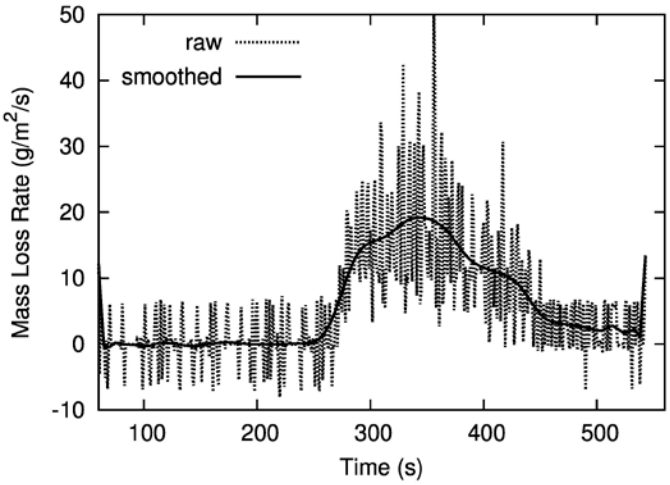

(a) Noise in MLR data

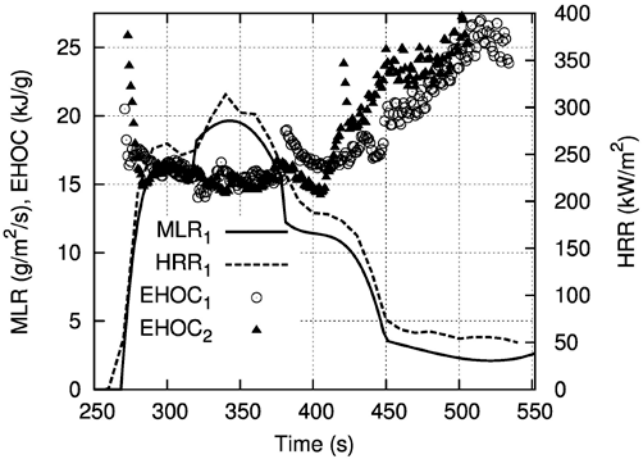

(b) HRR, Fitted MLR, and the EHOC

Figure 7. Graphical Representation of EHOC Calculation

Although char grew into the cone heater and ruined the mass recordings for both wet and dry samples, char buildup for wet samples was more severe. Thus, this study was performed using

data from dry samples. Accordingly, the EHOC of dry samples were chosen to be 16 kJ/g and 27 kJ/g for the first and second reactions, respectively. It was assumed that wet samples have higher combustion efficiency based on average cone EHOC data. Hence, the EHOC of wet samples for the first reaction was set as 20 kJ/g.

Heat of Reaction. The heat of fusion for PEEK is 130 J/g [12, 13, and 32]. After adjusting for 35% crystallinity, the heat of reaction for equation 4 is 50 J/g. The heats of reaction for equations 5 and 6 are unknown. Since the main focus of the modeling study is time to ignition, and heats of reaction do not have any influence on this parameter, heats of reaction of the first and second reactions are chosen, arbitrarily, to be 350 J/g and 0 J/g, respectively.

Char Yield. The char yield for thick samples measured in cone calorimetry varied and was not consistent at different heat flux settings. This is partly due to the error in the mass recordings during the experiments. Especially for the wet samples, char buildup increased until char hit the cone heater and resulted in erroneous mass readings. This difficulty was circumvented by using thinner samples for which char did not grow into the cone heater. For 1-mm-thick samples tested at 50 kW/m^2, the char yield, μ, was calculated to be 0.5, consistent with the char yield obtained from MCC and TGA.

To prevent thinner samples from coming off the frame, they were initially secured by means of wires across the sample face. In the cone calorimetry experiments using wireframes for 1-mm-thick samples, tested at 50 kW/m^2, caused scatter in peak heat release rate (PHRR) values. Thus, tests were performed using standard edge frames.

SUMMARY OF MODEL PARAMETERS.

Respectively, tables 5 and 6 show the material properties and reaction parameters used in the model. The density of the char is specified proportional to the virgin polymer and the corresponding char yield for numerical reasons to keep the volume of the material constant throughout the computation, and to avoid the computational burden of regridding [10]. The specific heat capacity is set equal to that of graphite and is adjusted using estimated char density. The properties of the insulation material (Kaowool) are assumed to be similar to a blanket.

Table 5. Model Material Properties

	P	P_{MELT}	P_{BUBBLE}	$Char_{A/B}$	Kaowool
ρ (kg m^{-3})	1300	1300	1300	ρ_P x $\mu_{A/B}$	48
c_P (J kg^{-1} K^{-1})	795 +2.22 T	2160	1000	1720 x ρ_{Char} /$\rho_{Char\ model}$	800
k (J kg^{-1} K^{-1})	0.21 +1.26 10^{-4} T	0.29	0.06	0.05 +4.00 10^{-10} T^3	0.08
ε	1	0.84	1	1	0
α (m^2 kg^{-1})	1.5	1	1	100	1000

Table 6. Model Reaction Parameters

Reaction No.	A (1/s)	E_a (kJ/mol)	μ	H (J/g)	EHOC (kJ/g)
4	10^{-1}	0	N/A	50	N/A
5	10^{32}	557.4	0.62	350	16
6	10^{3}	89	0.88	0	27
6	10^{5}	146.5	0.88	0	27
7	10^{3}	129	N/A	0	27
8	10^{-1}	0	N/A	0	N/A
9	10^{32}	557.4	0.62	350	20

RESULTS

CONE CALORIMETRY TESTS.

Four main sets of cone calorimetry tests were conducted. In the first set, morphologies of the specimens with varying moisture contents were examined on 3.9-mm-thick samples subject to 50 kW/m^2 external heat flux (see the Visual Observations section). In the second set, surface temperatures were monitored for 3.9-mm-thick samples at 50 kW/m^2 (see the Surface Temperature Measurements section). Next, the critical heat flux of wet and dry samples were determined on 1-mm-thick samples, and confirmed on 3.9-mm-thick samples (see the Critical Heat Flux section). Last, the rates of heat release and mass loss were measured for 1- and 3.9-mm-thick samples at three external heat fluxes: 50, 70, and 90 kW/m^2 (see the HRR Measurements section).

VISUAL OBSERVATIONS. A specimen from each conditioning category (dry, ambient, and wet) was exposed to a heat flux of 50 kW/m^2 in the cone calorimeter. During the test, before ignition, specimen surfaces were monitored for any morphological changes. Upon ignition, specimens were removed from the sample post and fractured to examine possible morphological changes in the interior. Figure 8 (a-c) shows the surfaces facing the radiant heat source and the cross sections of dry, ambient, and wet samples, respectively.

There is a remarkable difference between the morphologies of wet and dry specimens. While the surface of the dry sample was glossy and smooth throughout the test duration, the wet sample started to bubble early. These bubbles increased in size and number as the ignition temperature was approached. The photograph of the dry-sample surface, shown on the left in figure 8 (a), was taken after ignition. The glossy, smooth part of the surface towards the edge where no char had yet formed was clearly visible. In fact, the dry specimen was transparent, reflecting the aluminum foil used underneath for insulation at the time when the sample post was first taken out. It became opaque while cooling down, as the temperature of the specimen dropped below the melting temperature of 343°C, i.e., as it underwent a transition from an amorphous to a crystalline state.

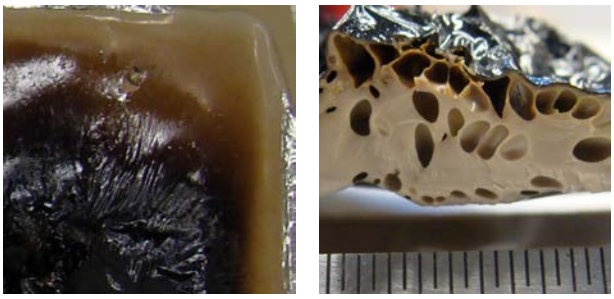

(a) Dry Sample

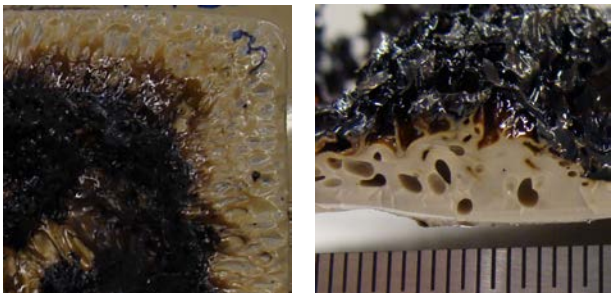

(b) Ambient Sample

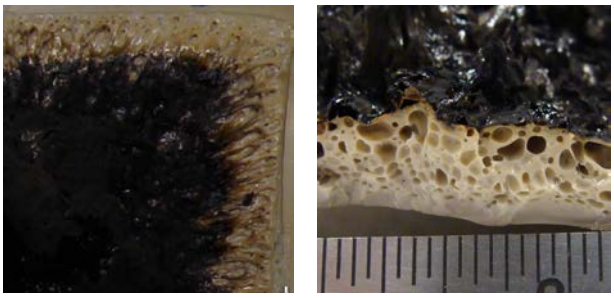

(c) Wet Sample

Figure 8. Specimen Surfaces (Left) and Cross Sections (Right)

On the other hand, the surface photographs of the wet and ambient samples display bubbles of varying sizes, shown in figure 8 (b and c). The lack of any surface perturbation for the dry samples is an indication that surface bubble formation is merely a consequence of water absorption. The increased number density for wet samples in comparison to the ambient samples also suggests a direct correlation between surface bubble formation and moisture content.

Although the surface of the dry polymer was smooth, its cross section, shown on the right in figure 8 (a), revealed bubbles of uniform size that had accumulated under the charred skin. A similar observation was also observed in the wet sample cross section shown on the right in figure 8 (c). The larger bubbles adjacent to the charred region diminished towards the back surface where there was a layer of virgin material in the sponge-like cross sections of wet specimens. Conversely, there were small bubbles lined up at this location for the dry specimen,

suggesting a deeper thermal penetration (see figure 8 (a)). Furthermore, the aluminum foil used around the samples as an insulation medium could not be easily removed from the dry sample. This also implies a difference in the temperature profiles for wet and dry samples and larger overall temperatures at the time of ignition for dry samples. However, it must be noted that the dry sample was subject to the heat exposure longer due to its delayed ignition time. Thus, a deeper thermal penetration must be expected.

It is obvious that there are two separate bubble formation mechanisms in effect for PEEK specimens—one is due to the thermal decomposition, and the other is the result of water evaporation. For the dry specimens, only the former mechanism plays a role since there is no moisture. Upon temperature rise, the chemical bonds start to break, yielding a decrease in molecular weight and viscosity of the polymer. Local temperature gradients in the molten polymer create bubble nucleation sites. Once the heat of vaporization is reached, the newly formed gas particles diffuse within the molten polymer and collect into bubbles. The bubbles do not escape from the surface immediately, but continue accumulating more gas constituents until the surface skin is ruptured by high-temperature volatiles [33 and 34]. For wet specimens, on the other hand, both of the bubble formation mechanisms act together. Upon exposure to heat, water molecules go through phase transition (at 100°C) but are trapped within the polymer until the polymer starts to liquefy (at the melting temperature of 343°C). At and above the melting temperature, however, steam (that is ready to escape) moves towards the less-viscous parts, i.e., towards the surface of the material and creates surface bubbles that grow with time. As the decomposition temperatures are reached, volatiles start diffusing into already existing nucleation sites. Since the bubble growth is limited by the number of neighboring bubbles, the number density increases and the bubble sizes decrease. The presence of moisture in the polymer alters the bubble nucleation and causes the high-number density small bubbles, presumably because of the rapid bubble formation as the trapped water vapor is suddenly able to expand when the polymer melts. In contrast, the release of volatile organic species will be much slower, leading to the formation of fewer, larger bubbles.

The bubble formation, shown in figure 9, continues to take place until all moisture leaves the specimen as water vapor. During the bubbling period, the specimen undergoes evaporation, and its morphology changes to affect its thermal properties. If thermal decomposition temperature is reached between t_{start} and t_{end}, the ignition time of the specimen will depend on the thermal properties of the bubbled surface. If, on the other hand, the sample has enough time to dry out before ignition, i.e., $t_{ign} > t_{end}$, its ignition mechanism will be dictated by the thermal properties of the dry sample. Although the moisture content has a greater impact at the lower heat fluxes, this is only true if the decomposition starts while bubbling takes place. Hence, the scatter in ignition time will be minimal for irradiation levels low enough to allow drying and high enough to shorten the bubbling period. Table 7 displays the average times bubbles are first observed in the experiments (note that this is actually when melting starts).

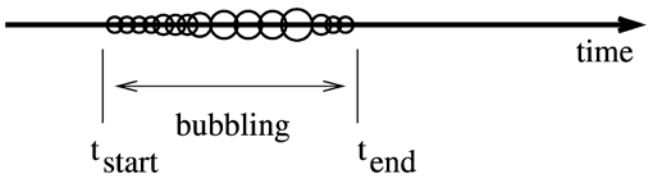

Figure 9. Schematic of Bubble Formation Period

Table 7. Times to Surface Bubble Formation

$\dot{q}''_{ext}$ (kW/m^2)	t_{start} (seconds)
50	40
70	24
90	15

SURFACE TEMPERATURE MEASUREMENTS. The surface temperature of 3.9-mm-thick samples exposed to 50 kW/m^2 external heat flux was measured using a thermocouple probe during irradiation, to understand the behavior leading to ignition delay for dry samples. The surface temperature variation is displayed in figure 10 for the wet and dry samples tested. There is no noticeable difference between the samples at the glass transition temperature T_g of 143°C. For wet samples, the bubble formation starts at the melting temperature T_m of 343°C. After melting, the dry sample surface heats up at a slower rate as the molten polymer allows more heat to be conducted into its bulk than the foamed (wet) polymer. The ignition temperature, T_{ign}, of 540°C is reached in 120 seconds for the wet sample when the dry sample surface is still 70°C cooler (470°C). The surface temperature of thicker samples, used to determine material properties (see the Material Properties section), are also measured with similar observations.

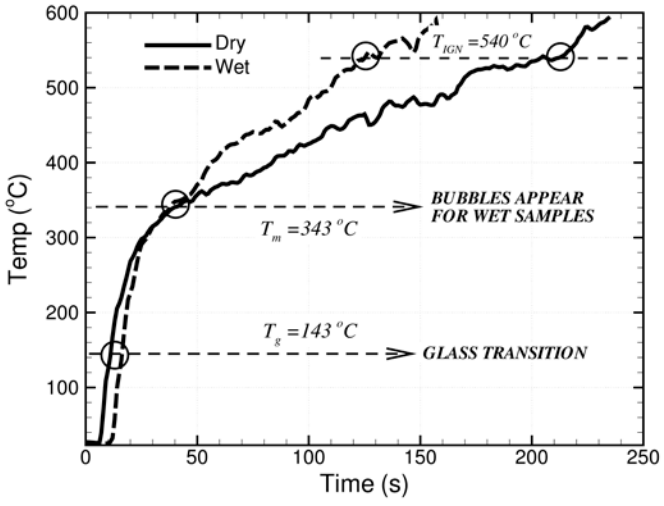

Figure 10. Surface Temperature Variation Before Ignition $\dot{q}''$ = 50 kW/m^2

CRITICAL HEAT FLUX. The critical heat flux was first determined on 1-mm-thick samples. The HRR histories of the experiments are shown in figure 11. In these tests, the edge frame was not used. The International Organization for Standardization standard [35] requires a 15-minute waiting period in the determination of the critical heat flux for piloted ignition. A longer period was used in the tests. A sustained, albeit weak, flame was observed even at 26 kW/m^2. However, it was not possible to reproduce the flaming in the repeated tests of 25 and 27 kW/m^2. The HRR obtained at an external heat flux of 27 kW/m^2 is ~70 kW/m^2, as shown in figure 11(a). This value is consistent with the critical HRR, characterizing sustained ignition [28]. Thus, the minimum heat flux that led to sustained ignition for PEEK was found to be between 27 and 30 kW/m^2.

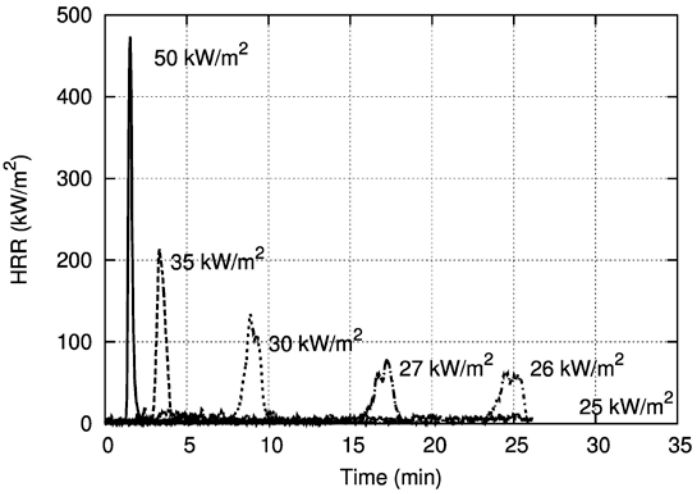

(a) HRR at Different Irradiation Levels

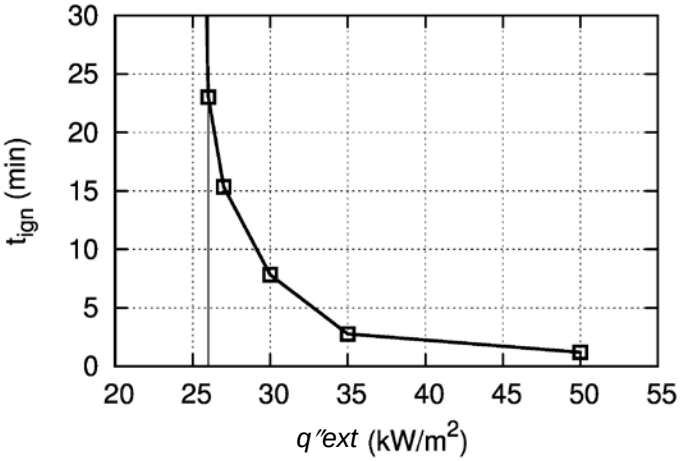

(b) Times to Ignition at Different Irradiation Levels

Figure 11. Determination of Critical Heat Flux on a 1-mm-Thick Sample From Asymptote of Ignition Delay

Materials can be grouped in terms of their thermal behavior; thermally thick materials are those for which the heat losses from the back face is negligible and semi-infinite slab assumption is

valid, whereas the thermally thin materials are those with negligible temperature gradients over their thickness [31]. The characteristic thermal conduction length can be used in relation to the actual physical thickness, L, to determine the type of the material studied. It is proportional to the square root of the thermal diffusivity, α = k/ρc, and the exposure time, t, as $\sqrt{\alpha \cdot t}$. The material is considered thermally thick if $L > 4\sqrt{\alpha \cdot t}$, and thermally thin if $L < \sqrt{\alpha \cdot t}$ [31]. In this study, the characteristic thermal conduction length is calculated to be ~0.32 $\sqrt{t}$ mm using the material properties listed in table 1. This means that the 3.9-mm-thick specimen, subjected to these irradiation levels, does not behave as a thermally thick material at the time of ignition ($3.9 < 4 * 0.32\sqrt{t_{ign}}$). Thus, for the 3.9-mm wet and dry samples, the thermally thin material ignition theory was followed. Figure 12 shows the reciprocal variations of the ignition time with the external heat flux. Based on the ignition time calculations for the thermally thin materials, the slopes of these curves correspond to $1/\rho\ c_p\ l\ (T_{ign}-T_\infty)$ [36]. Since the critical heat flux converges as the ignition time goes to infinity, the intercept of the curves indicates the critical heat flux below which ignition is not possible. This is, of course, only an approximate theoretical lower limit. The linear behavior is not expected to hold close to the critical heat flux that can only be reached asymptotically. However, it is reasonable to assume that the critical heat flux lies between 25 to 30 kW/m^2. Over the three heat fluxes of this study, a linear fit to the test data yields $10^3/t_{ign_{WET}} = 0.35\ \dot{q}''_{ext} - 8.6$ for the wet samples and $10^3/t_{ign_{DRY}} = 0.25\ \dot{q}''_{ext} - 8$ for the dry samples. Accordingly, assuming the same ignition temperature for wet and dry samples, in agreement with the surface temperature measurements (figure 10), the ratio of $(\rho\ c_p\ l)_{wet}/(\rho\ c_p\ l)_{dry}$ is ~0.7. This shows that moisture uptake decreases the ignition time by decreasing the thermal heat capacity.

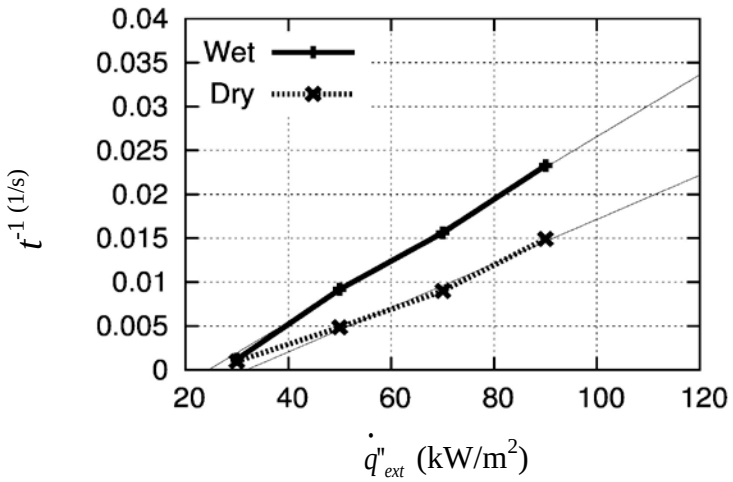

Figure 12. The Variation of Reciprocal Time to Ignition With External Heat Flux for 3.9-mm-Thick Wet and Dry Samples

The virgin material adjacent to the back face in the cross-sectional photographs of wet samples (figure 8 (c)) is a clear indication that the assumption of thermally thin material does not hold for wet samples as a whole. However, we consider that only a film of material above the bubbled surface is responsible for fuel generation leading to ignition for wet samples; therefore, thermally-thin ignition theory is still applicable.

HEAT RELEASE MEASUREMENTS. The burning behavior of materials is usually characterized by a set of fire performance parameters including time to ignition (t_{ign}), total burn time (t_{burn}), peak HRR (PHRR), time to PHRR (t_{PHRR}), average HRR (AHRR), and THR. In this section, the cone calorimetry test data of 3.9-mm specimens is examined to quantify the differences in burning behavior of wet and dry samples by scrutinizing the fire performance parameters.

The cone tests were conducted in triplicate at each of the three heat flux settings (50, 70, and 90 kW/m^2); there are 18 experiments reported. Table 8 shows t_{ign}, t_{burn}, t_{PHRR}, PHRR, and THR obtained from the cone experiments, and are averaged for the wet and dry samples. The wet samples consistently ignited earlier than the dry samples, while this delay in ignition decreased as the external heat flux was increased. The difference in t_{ign} between wet and dry samples was more than 1.5 minutes (97 s) for $\dot{q}''_{ext}$ = 50 kW/m^2, while it was less than half a minute (24 seconds) for $\dot{q}''_{ext}$ = 90 kW/m^2. The total burn time, defined as the time period between ignition and flameout, was longer for the wet samples, suggesting a slower burning rate compared to the dry samples, presumably because less heat was absorbed prior to ignition. Furthermore, the dry samples produced higher HRR in a shorter time as evidenced from the tabulated PHRR and t_{PHRR} values. Note that, although t_{PHRR} values of wet and dry samples are comparable, once ignition takes place, t_{PHRR} is shorter for dry samples due to longer ignition times. It is interesting to see variation in THR that exists not only between wet and dry samples, but also in each category. The THR was smaller for low heat flux tests, indicating the presence of unburned material at the end of the test.

Table 8. Average Test Data for 3.9-mm Samples at $\dot{q}''_{ext}$ = 50, 70, and 90 kW/m^2

Type	$\dot{q}''_{ext}$ (kW/m^2)	t_{ign} (seconds)	t_{burn} (seconds)	t_{PHRR} (seconds)	PHRR (kW/m^2)	THR (MJ/m^2)
Dry	50	207	164	300	355	46
	70	111	168	197	387	48
	90	68	165	151	504	62
Wet	50	110	247	315	280	54
	70	65	211	180	351	63
	90	44	200	157	377	65

(a) Wet Samples

The HRR histories for the 3.9-mm-thick dry and wet specimens are plotted in figure 13 (a and b), respectively. The average of the HRR at each heat flux setting is shown with a thicker line and symbols in the figure. The sample subjected to a heat flux of 90 kW/m^2 ignites earlier with a higher PHRR. The observed ignition mechanism was different for the wet and dry samples. Wet samples, having a permeable surface, allowed volatiles to escape through the sample surface, whereas dry samples formed a skin under which hot gases accumulated until there was enough pressure buildup to burst through the skin. This sudden gas release can be seen as a spike (or a shoulder) at t_{ign} in the HRR plots of the dry samples (figure 13 (a)). On the other hand, the HRR curves of the wet samples are smoother due to the porous surface, allowing both moisture and volatiles to escape easily and burning to take place steadily (figure 13 (b)). At lower heat fluxes, the HRR curves of wet samples resemble those of the thermally thick materials.

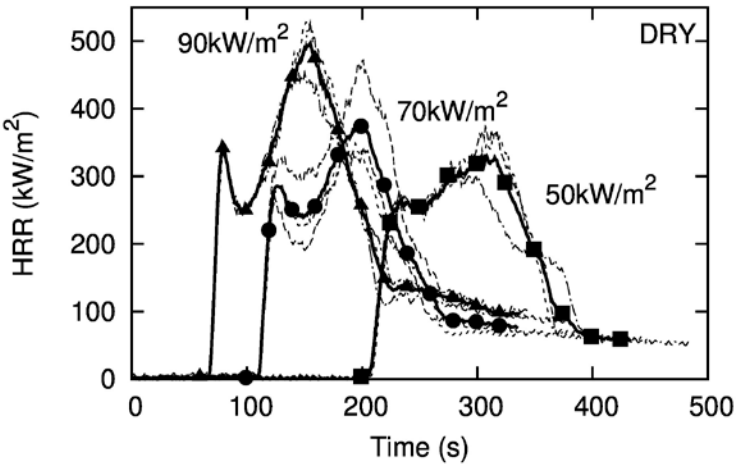

(a) Dry Samples

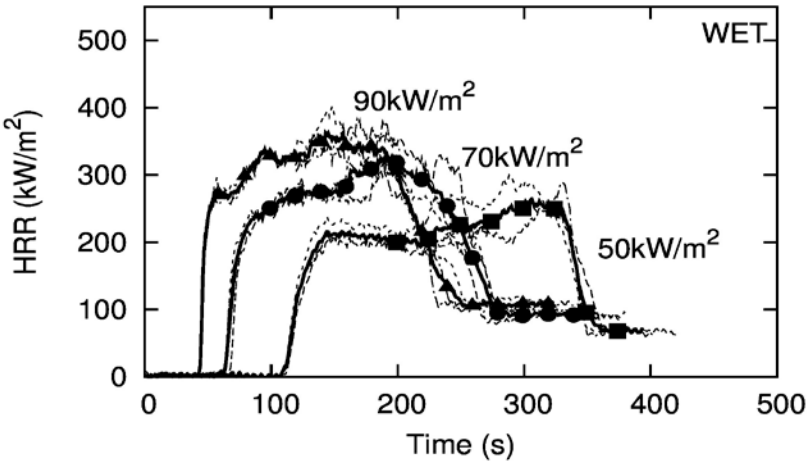

(b) Wet Samples

Figure 13. Cone Calorimetry Data: HRR Histories for 3.9-mm-Thick Samples

PYROLYSIS MODELING.

The effect of moisture uptake on the fire performance parameters of PEEK is clear from the experimental data shown in figure 13 (a and b); in comparison to the dry specimens, wet specimens have shorter t_{ign}, longer t_{burn}, and lower AHRR and PHRR. The experimental data and observations suggest that, depending on the level of moisture content prior to ignition, the material properties of PEEK change in relation to its morphological state. Thus, it seems that the differences in the burning behavior of wet and dry samples are due to a physical phenomenon rather than a chemical one. Therefore, in the modeling efforts, wet and dry samples are treated exactly the same except for the change in the preignition material properties representing the physical formation of bubbles for wet specimens.

Besides having shorter t_{ign} than dry samples, wet samples have lower PHRR and longer t_{burn}. In other words, the impact of moisture is observed in two seemingly distinct ways: (1) polymer ignites faster (i.e., its surface heats up quicker) and (2) burning takes longer, (i.e., its temperature increases gradually). There are several scenarios that may lead to these physical phenomena. One scenario is that the bubbles formed on the surface of the wet samples create an insulating layer that serves as a barrier for the underlying material. The foamed up surface acts as a material with low conductivity and yields a slower temperature rise within the material than its surface. A second scenario is that the optical properties of the specimen alter due to surface bubble formation. This newly formed, thin layer hinders the in-depth absorption and causes irradiation to be absorbed on the surface.

Based on these two hypotheses, a calculation was performed where the conductivity and heat capacity of the polymer melt is decreased drastically to account for the low thermal conductivity and heat capacity of the bubbles and all radiation is absorbed on the surface (the in-depth radiation is turned off). The conductivity and heat capacity of the molten state are determined by fitting model results to the cone calorimetry temperature data for 10-mm-thick wet samples (see figure 4 (b)).

Model predictions and experimental observations for ignition delays are compared in table 9 for both wet and dry samples. The experimental values listed in the table are based on three separate experiments for each external heat flux and thickness studied. Although experimental data scatter in ignition times for 3.9-mm-thick specimens are negligible, there is more than a 10-second difference for both 1- and 10-mm specimens. Note that material properties are determined by fitting the experimental data of 10-mm specimens. For all cases studied, the model ignition delays are within experimental uncertainty and well-predicted. The ignition time estimates of dry samples are close to the test data. However, ignition time for wet samples is estimated to be approximately 10 seconds late at 50 kW/m^2, and 10 seconds early at the higher heat flux settings.

Figure 14 (a, c, and e) and figure 14(b, d, and f) show HRR obtained from the numerical model for a 3.9-mm-thick sample along with the cone calorimetry data at external heat fluxes of 50, 70, and 90 kW/m^2 for dry and wet samples, respectively (dotted lines with symbols show the average of the three experiments for each heat flux). The model predictions are good at capturing t_{ign} (as

shown in table 9) and t_{burn}. Moreover, the general shape of the HRR curves compare well with the test data. Not only are the PHRR predictions within the uncertainty of experimental data and well-predicted, but the t_{PHRR} estimates are close to the corresponding test data at different heat fluxes for dry samples (tables 8 and 10). Furthermore, the tails of the HRR curves associated with the char oxidation are in agreement with the experiments except for the slight difference observed at 50 kW/m^2 for dry samples, whereas the PHRR at high heat flux settings are higher than the experimental data, and the HRR tails are underestimated for wet samples (table 10).

Table 9. Comparison of Model Ignition Delays (t_{ignM}) With Test Data (t_{ignE})

Type	$\dot{q}''_{ext}$ (kW/m^2)	Thickness (mm)	t_{ignM} (seconds)	t_{ignE} (seconds)
Dry	50	1	75	72-90
Dry	50	3.9	202	205-209
Dry	70	3.9	105	110-113
Dry	90	3.9	65	68
Dry	50	10	365	350-390*
Wet	50	3.9	126	108-113
Wet	70	3.9	55	64-67
Wet	90	3.9	34	43-44
Wet	50	10	180	130-185*

* fitted data

Table 10. Model Predictions for 3.9-mm Samples

Type	$\dot{q}''_{ext}$ (kW/m^2)	t_{burn} (seconds)	t_{PHRR} (seconds)	PHRR (kW/m^2)	THR (MJ/m^2)
Dry	50	162	280	250	41
	70	175	200	350	50
	90	165	150	460	60
Wet	50	224	340	250	49
	70	225	200	375	59
	90	216	160	500	65

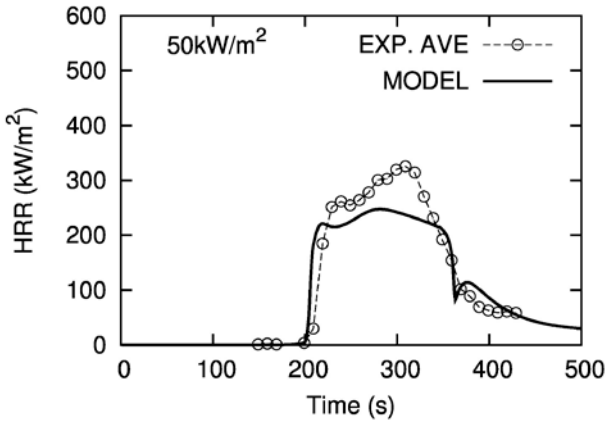

(a) Dry Sample at $\dot{q}''_{ext}$ = 50 kW/m^2

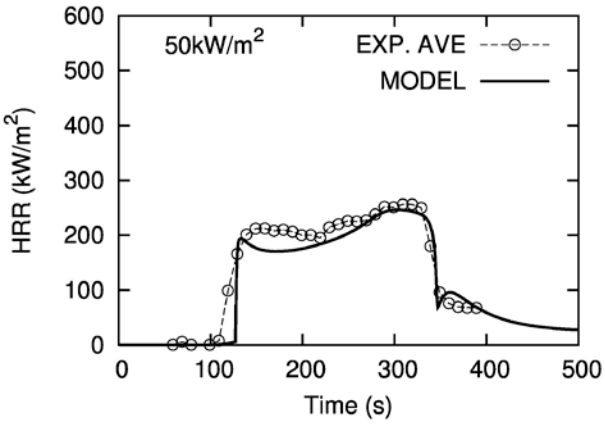

(b) Wet Sample at $\dot{q}''_{ext}$ = 50 kW/m^2

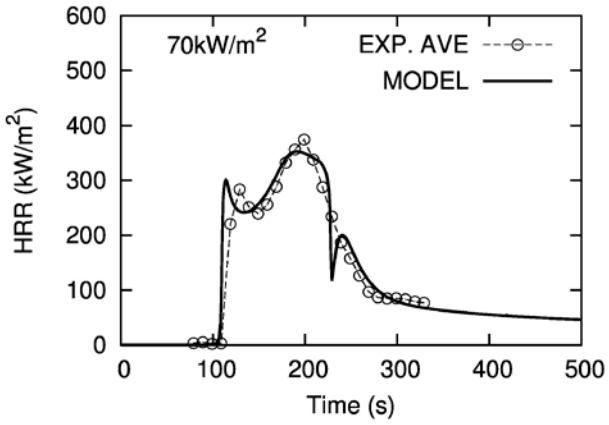

(c) Dry Sample at $\dot{q}''_{ext}$ = 70 kW/m^2

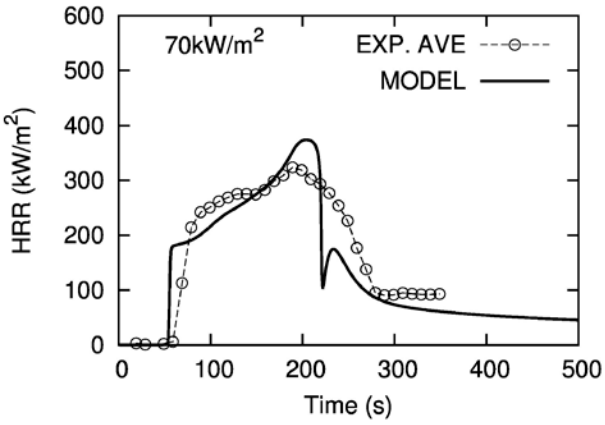

(d) Wet Sample at $\dot{q}''_{ext}$ = 70 kW/m^2

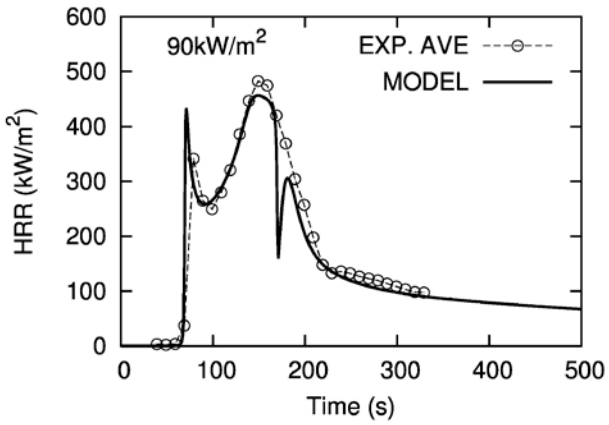

(e) Dry Sample at $\dot{q}''_{ext}$ = 90 kW/m^2

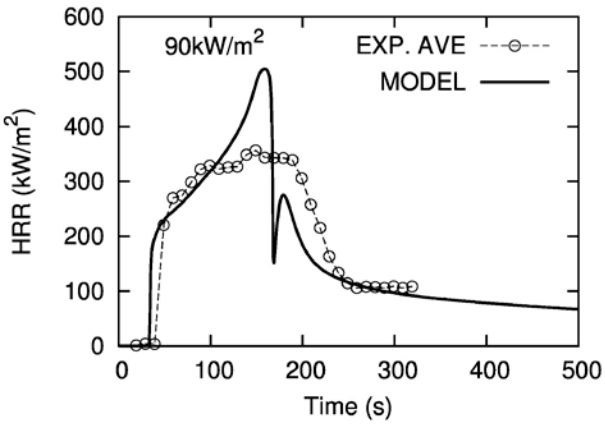

(f) Wet Sample at $\dot{q}''_{ext}$ = 90 kW/m^2

Figure 14. Comparisons of HRR Predictions With the Average Cone Data for Dry and Wet Samples

The time variations of mass loss for dry and wet samples are shown in figure 15 (a and b), respectively. Consistent with the above observations, both mass loss histories are well-estimated by the model. Note that because of the char swelling into the cone heater, mass loss data for the wet samples are not complete. For the low external heat flux of 50 kW/m^2, the char yield value of 0.48 was not reached in both the wet and dry specimen experiments. This is consistent with the low THR calculation at this heat flux setting. Figure 16 (a and b) displays the THR histories for dry and wet samples, respectively. THR histories are well-estimated by the model except for the THR at 70 kW/m^2, which has high experimental uncertainty and model results fall between the test data. Note that, in comparison to the dry samples, THR of wet samples are higher in agreement with the experimental data (tables 8 and 10).

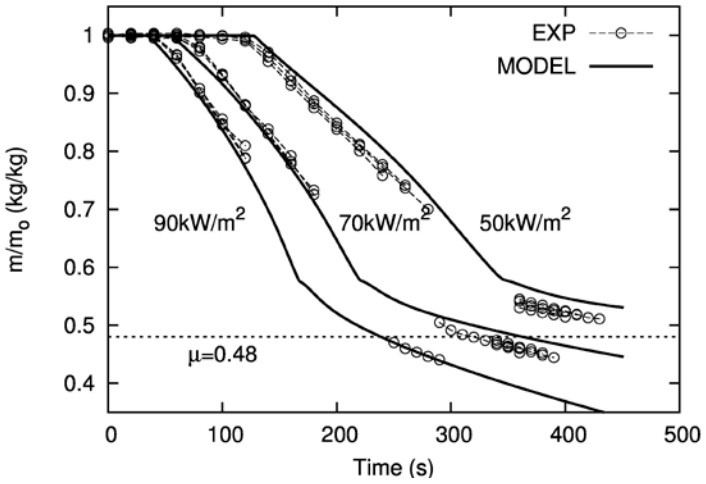

(a) Wet Samples

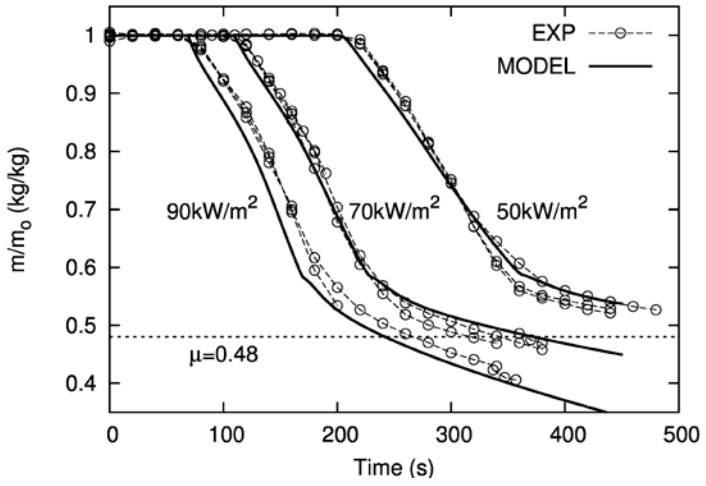

(b) Dry Samples

Figure 15. Comparisons of Model Predictions With the Test Data: Mass Loss Histories

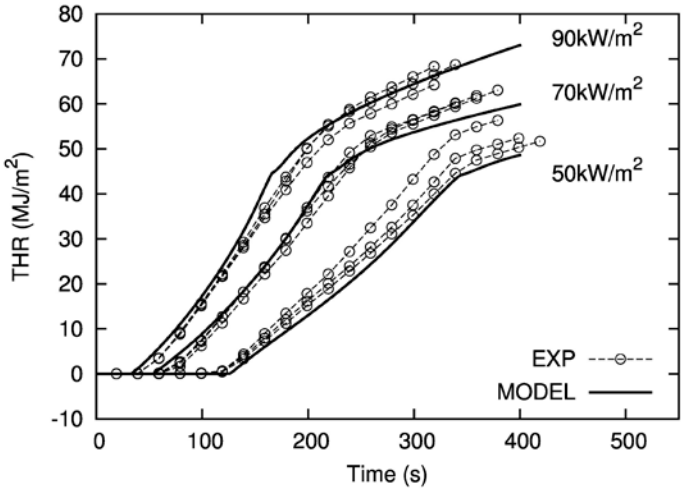

(a) Wet Samples

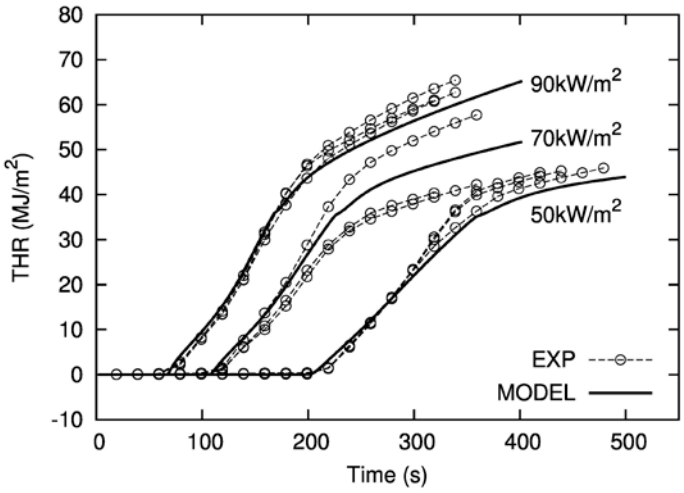

(b) Dry Samples

Figure 16. Comparisons of Model Predictions With the Test Data: THR Histories

Charring, yielding a carbonaceous residue, is an important physical change for materials undergoing thermal decomposition. Since the char layer shields the underlying virgin material from the heat source, the decomposition rate decreases as char builds up. However, in the cone calorimetry tests of PEEK, as the charring material swells to the cone heater, the heat exposure at the char surface increases. The effect of charring, as a barrier for the virgin material or as an extended surface to the cone heater, is not taken into account in the model; i.e., external heat flux is assumed to be constant throughout the model and not adjusted for charring.

SUMMARY AND CONCLUSIONS

Sources of variability in relation to the environmental conditions were examined for the bench scale fire tests of a high-performance thermoplastic, poly(aryl ether ether ketone) (PEEK). More specifically, the effect of moisture absorption on the burning behavior of PEEK was evaluated following an earlier work where the fire response of this polymer was found to be sensitive to humidity. The PEEK samples were studied in two groups that were conditioned as wet and dry. The thermal degradation of the polymer was investigated using cone calorimetry and thermal analysis techniques. In addition to the ignition characteristics, heat release rate (HRR) and mass loss histories were assessed for wet and dry specimens. The experimental investigation was followed by a numerical study to understand the processes behind the variation observed in the burning characteristics. A one-dimensional pyrolysis modeling tool, ThermaKin, was used to model cone calorimetry tests of dry- and wet-PEEK specimens.

The surface temperature measurements and the visual observations were consistent with a burning morphology of the polymer that depended on the moisture content of the tested specimen. Particularly, the size and the number density of the bubbles in degraded polymer were clearly correlated with the moisture absorption levels. The lower ignition times and HRR of the wet specimens were the direct consequences of different bubble nucleation and growth mechanisms in wet and dry samples. Not only did bubble dynamics play an important role in the transport of gaseous decomposition products, but they also altered the optical and thermal properties of the polymer. These findings confirmed the significance of environmental conditions and suggested a standardization procedure for test specimens.

In the modeling of the wet samples, a new reaction for the bubble formation was defined. Based on the experimental observations, the moisture content was represented by conductivity, heat capacity, absorptivity, and reflectivity of the bubbled polymer in the model. The conductivity and the heat capacity were determined by the surface temperature measurements. The predicted time to ignition for both wet and dry samples, which was the main focus of this study, agreed very well with the results of the experiments. Furthermore, the predictions of the HRR, mass loss, total heat release, and the individual fire performance parameters compared well with the cone data. However, it is important to note that model results after ignition depend greatly on a number of parameters that are not known. These included, but were not limited to, thermal and optical properties of the char, heat of decomposition reaction, flame heat flux, and variations of the external heat flux due to char swelling. Future work to quantify the effects of these sources of uncertainty in the determination of the fire performance properties is needed for better and more reliable model predictions beyond time to ignition. This fact, however, does not invalidate the numerical analysis presented since the relative difference in the burning behavior between wet and dry samples was elaborated on rather than the most accurate representation of one selected state (dry or wet). Using the same value for the unknown quantities in the modeling of both wet and dry samples made it possible to investigate the changes in postignition burning behavior due to moisture uptake, which may be driven by the same physical phenomena that yield the ignition time scatter.

REFERENCES

1. Patel, P., "Investigation of Fire Behaviour of PEEK-Based Polymers and Compounds," PhD Thesis, University of Central Lancashire, United Kingdom, 2011.

2. Sims, D.L. and Law, M., "The Ignition of Wet and Dry Wood by Radiation, Combustion and Flame," Vol. 11, Issue 5, 1967, pp. 377-388.

3. Lee, C.K. and Diehl, J.R., "Combustion of Irradiated Wet and dry Oak, Combustion and Flame," Vol. 42, 1981, pp. 123-138.

4. Galgano, A. and Di Blasi, C., "Modeling the Propagation of Drying and Decomposition Fronts in Wood," *Combustion and Flame*, Vol. 139, 2004, pp. 16-27.

5. Khan, M., De Ris, J.L., and Ogden, S.D., "Effect of Moisture on Ignition Time of Cellulosic Materials," *Fire Safety Science, Proceedings of 9th International Symposium*, 2008, pp. 167-178.

6. Material Properties Guide, www.victrex.com.

7. Atreya, A., "Ignition of Fires," *Philosophical Transactions of the Royal Society A: Mathematical, Physical & Engineering Sciences*, Vol. 356, No. 1748, 1998, pp. 2787-2813.

8. Stoliarov, S.I. and Lyon, R.E., "Thermo-Kinetic Model of Burning," Federal Aviation Administration Technical Note, DOT/FAA/AR-TN08/17, 2008, www.fire.tc.faa.gov /reports /reports.asp.

9. Stoliarov, S.I. and Lyon, R.E., "Thermo-Kinetic Model of Burning for Pyrolyzing Materials," *Proceedings of the 9th International Symposium on Fire Safety Science*, 2009, pp. 1141-1152.

10. Stoliarov, S.I., Crowley, S., Walter, R.N., and Lyon, R.E., "Prediction of the Burning Rates of Charring Polymers," *Combustion and Flame*, Vol. 157, Issue 11, November 2010, pp. 2024-2034.

11. Hsiao, B., Gardner, K.H., Wu, D.Q., and Chu, B., "Time-Resolved X-ray Study of poly(aryl ether ether ketone) Crystallization and Melting Behaviour: 1. Crystallization," *Polymer*, Vol. 34, No. 19, 1993, pp. 3986-3995.

12. Blundell, D.J. and Osborn, B.N., "The Morphology of Poly(aryl-ether-ether-ketone)," *Polymer*, Vol. 24, Issue 8, August 1983, pp. 953-958.

13. Kemmish, D.J. and Hay, J.N., "The Effect of Physical Ageing on the Properties of Amorphous PEEK," *Polymer*, Vol. 26, Issue 6, June 1985, pp. 905-912.

14. Nguyen, H.X. and Ishida, H., "Poly(aryl-ether-ether-ketone) and Its Advanced Composites: A Review," *Polymer Composites*, Vol. 8, Issue 2, April 1987, pp 57-73.

15. Day, M., Suprunchuk, T., Cooney, J.D., and Wiles, D.M., "Thermal Degradation of Poly(aryl-ether-ether-ketone) (PEEK): A Differential Scanning Calorimetry Study," *Journal of Applied Polymer Science*, Vol. 36, Issue 5, August 1988, pp. 1097-1106.

16. Jones, A. and Legras, R., "Thermal Stability and Crystallization of Poly(aryl ether ether ketone)," *Polymer*, Vol. 32, Issue 15, 1991, pp. 2691-2706.

17. Zhang, Z. and Zeng, H., "Effects of Thermal Treatment on Poly(ether ether ketone)," *Polymer*, Vol. 34, Issue 17, 1993, pp. 3648-3652.

18. Chen, J.Y., Chen, M., and Chao, S.C., "Thermal Stability and Crystallization Kinetics of Poly(ether ether ketone)," *Macromolecular Chemistry and Physics*, Vol. 199, Issue 8, August 1998, pp. 1623-1629.

19. Perng, L.H., Tsai, C.H., and Ling, Y.C., "Mechanism and Kinetic Modeling of PEEK Pyrolysis by TG/MS," *Polymer*, Vol. 40, Issue 26, 1999, pp. 7321-7329.

20. Lu, S.X., Cebe, P., and Capel, M., "Thermal Stability and Thermal Expansion Studies of PEEK and Related Polyimides," *Polymer*, Vol. 37, Issue 14, July 1996, pp. 2999-3009.

21. Patel, P., Hull, T.R., McCabe, R.W., Flath, D., Grasmeder, J., and Percy, M., "Mechanism of Thermal Decomposition of Poly(ether ether ketone) (PEEK) From a Review of Decomposition Studies," *Polymer Degradation and Stability*, Vol. 95, Issue 5, 2010, pp. 709-718.

22. Patel, P., Hull, T.R., Lyon, R.E., Stoliarov, S.I., Walter, R.N., Crowley, S., and Safronava, N., "Investigation of the Thermal Decomposition and Flammability of PEEK and Its Carbon and Glass-Fibre Composites," *Polymer Degradation and Stability*, Vol. 96, Issue 1, 2010, pp. 12-22.

23. Tewarson, A., *Flammability of Polymers*, "Chapter 11 in Plastics and the Environment," A.L. Andrady (editor), John Wiley and Sons, Inc., Hoboken, New Jersey, 2003.

24. Lyon, R.E., *Plastics and Rubber*, "Chapter 3 in Handbook of Building Materials for Fire Protection," C.A. Harper (editor), McGraw-Hill, New York, 2004.

25. ASTM Standard D618-08, "Standard Practice for Conditioning Plastics for Testing," ASTM International, West Conshohocken, Pennsylvania, 2008.

26. ASTM Standard D7309-07a, "Standard Test Method for Determining Flammability Characteristics of Plastics and Other Solid Materials Using Microscale Combustion Calorimetry," ASTM International, West Conshohocken, Pennsylvania, 2007.

27. ASTM Standard E1354-10a, "Standard Test Method for Heat and Visible Smoke Release Rates for Materials and Products Using an Oxygen Consumption Calorimeter," ASTM International, West Conshohocken, Pennsylvania, 2010.

28. Lyon, R.E. and Quintiere, J.G., "Criteria for Piloted Ignition of Combustible Solids," *Combustion and Flame*, Vol. 151, Issue 4, December 2007, pp. 551-559.

29. Beyler, C.L. and Hirschler, M.M., "Thermal Decomposition of Polymers," *SFPE Handbook of Fire Protection Engineering (3rd Ed)*, Section 1, Chapter 7, 2001, pp. 1-110.

30. Gronli, M.G., Varhegyi, G., and Di Blasi, C., "Thermogravimetric Analysis and Devolatilization Kinetics of Wood," *Industrial & Engineering Chemistry Research*, Vol. 41, Issue 17, 2002, pp. 4201-4208.

31. Drysdale, D., *An Introduction to Fire Dynamics*, John Wiley and Sons, Inc., Hoboken, New Jersey, 2002.

32. Seguela, R., "Temperature Dependence of the Melting Enthalpy of Poly(ethylene terephthalate) and Poly(aryl-ether-ether-ketone)," *Polymer*, Vol. 34, Issue 8, 1993, pp. 1761-1764.

33. Butler, K., "Physical Modeling of Intumescent Fire Retardant Polymers, Polymeric Foams," *ACS Symposium Series 669*, 1997, pp. 214-230.

34. Kashiwagi, T. and Ohlemiller, T.J., "A Study of Oxygen Effects on Nonflaming Transient Gasification of PMMA and PE During Thermal Irradiation," *19th Symposium on Combustion*, Combustion Institute, 1982, Vol. 19, Issue 1, pp. 815-823.

35. ISO Standard. "ISO 5657, Reaction to Fire-Ignitability of Building Products Using a Radiant Heat Source," International Organization for Standardization, Geneva, December 1997.

36. Quintiere, J.G., *Fundamentals of Fire Phenomena*, John Wiley and Sons, Inc., Hoboken, New Jersey, 2006.